Article

Stability Analysis of Open-Loop V/Hz Controlled Asynchronous Machines and Two Novel Mitigation Strategies for Oscillations Suppression

Lorenzo Carbone, Simone Cosso [ID]**, Krishneel Kumar** [ID]**, Mario Marchesoni ***[ID]**, Massimiliano Passalacqua** [ID]
and Luis Vaccaro [ID]

Department of Electrical, Electronic, Tlc Engineering and Naval Architecture (DITEN), University of Genova, via all'Opera Pia 11a, 16145 Genova, Italy; lorenzo.carbone@edu.unige.it (L.C.); simone.cosso@edu.unige.it (S.C.); krishneel.kumar@edu.unige.it (K.K.); massimiliano.passalacqua@unige.it (M.P.); luis.vaccaro@unige.it (L.V.)
* Correspondence: marchesoni@unige.it

Abstract: Asynchronous machines are always widely used in most industrial applications due to their reliability, flexibility, and manoeuvrability. To achieve variable speed operations, the quite simple open-loop V/Hz control is largely utilized. Under open-loop V/Hz control, the nonlinear interaction is well known to cause current and torque oscillations while operating at low to medium speeds under light loads. This article presents the stability analysis of induction motors at low–medium frequencies under no-load conditions with the V/Hz control. A system representation in the form of state space is discussed, and the region of instability is plotted against the V/f plane. Two novel and refined methods for the mitigation of oscillations in the region of instability are presented. The two proposed algorithms are finally tested and validated through simulation on an inverter-fed induction motor drive system.

Keywords: instability; eigenvalues; oscillations; V/Hz control; stability analysis; active damping; small-signal model; induction motor drive

1. Introduction

Induction motors are the most suitable choice in different fields of application, from low to high power [1]. The use of variable speed asynchronous motor drives has been existent since the early 1960s. This was made possible due to the development and the technology improvement in various power semiconductor devices [2,3]. In order to utilize induction machines in variable speed functions, efficient speed control techniques need to be adopted [4]. Compared to speed feedback-based techniques such as Field Oriented Control (FOC), open-loop V/Hz control has the advantages of low cost, ease of implementation, and a wide range of operating speeds; on the other hand, closed-loop controls like FOC can offer higher performance and better dynamic behavior, by controlling separately the flux and the current producing the torque. In addition, considering an open loop V/Hz control, a speed sensor is not required, since there is not a need for the speed measure. Therefore V/Hz inverter controls are widely used in adjustable speed applications including pumps, blowers, fans, etc. [5]. It is well known from the technical literature that V/Hz controlled PWM inverter-fed induction motor drives exhibit undesirable sustained oscillations in mechanical torque and stator currents [6–8]. These oscillations are caused by the interaction of the electrical and the mechanical subsystems (Figure 1), which are nonlinearly coupled through the electromagnetic torque and the back-electromotive force and are affected by changes in motor parameters. Hence, many studies can be found in the literature where the effects of motor and inverter parameters such as stator resistance, leakage inductance, rotor moment of inertia, DC-link capacitor, inverter dead time, switching frequency, and the number of poles are thoroughly analyzed [9]. In [7] a small signal linearized representation

is used to carry out a stability analysis of induction motors fed by a pure sinusoidal voltage source of adjustable amplitude and frequency, while inverter dead-time effect and modeling is considered in [10,11] and represented as an equivalent resistance in [12]. Recently, a more accurate method considering dead times is presented in [13], which demonstrates the oscillations leading the system to instability on the voltage versus frequency (V–f) plane. In the last decades, a few strategies have been proposed in order to suppress these oscillations. Some of these methods eliminate instability by modulating the inverter frequency in reaction to the current fluctuations on the DC-link as highlighted in [14], whereas in [15] a voltage vector feedback loop is implemented to counteract the effect of the leakage inductance and the stator resistance. Two very efficient active damping methods based on a dynamic current feedback have been presented in [16,17], which allow a significant reduction in the oscillations. In this article an accurate system representation in the state space is derived in order to perform stability analysis of induction machines at low–medium frequencies under no load conditions using the V/Hz control. The region of instability obtained from this stability analysis is plotted in the V–f plane. Two mitigation techniques are proposed with the aim of reducing the oscillations and avoiding instability; the first, which is an innovative strategy, is derived from creating a customized slope ramp of the V/Hz references, whereas the second is a variation of the active damping method presented in [16]. The two proposed algorithms are finally tested and validated through simulation on an inverter-fed induction motor drive system implemented in MATLAB/Simulink.
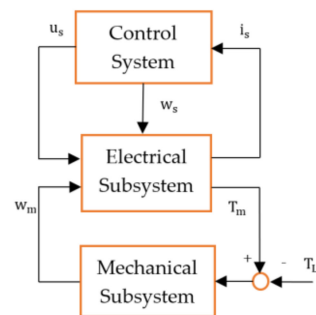

Figure 1. System architecture block diagram.

2. The Conventional V/Hz Control

The popular V/Hz control or the Voltage/Frequency control is a type of speed control adopted to enable induction motors to be used in variable speed applications. It is a speed control strategy where the output voltage frequency and amplitude are proportional. This is done to ensure that the motor flux is constant, which prevents the phenomenon of weak magnetic and magnetic saturation situations [18]. Figure 2 illustrates the conventional V/Hz control of an induction motor fed by a voltage source PWM inverter.
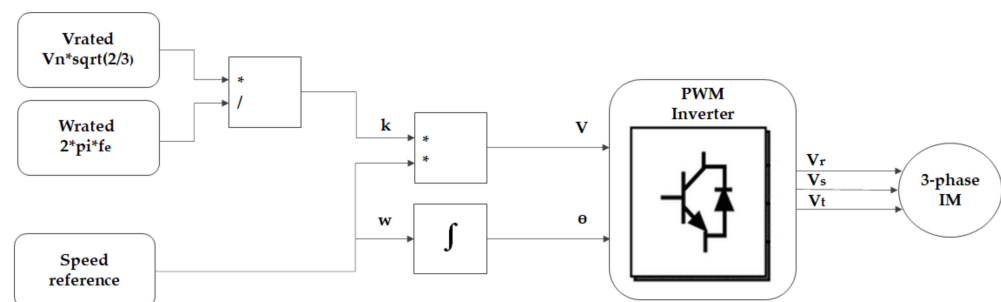

Figure 2. Conventional V/Hz control strategy block diagram.

The inputs to the inverter are the voltage calculated from the V/Hz logic and θ, which is obtained from the integration of the reference speed. K is equal to $\frac{V_n \sqrt{2/3}}{2\pi f_e}$, while w

represents the speed profile imposed. Table 1 lists all the induction motor drive (High Power) parameters, which were utilized henceforth for the simulations.

Table 1. Motor parameters.

Motor Parameter	Parameter Value
V_n—Nominal voltage	6.6 kV
I_n—Nominal current	75.8 A
I_m—Magnetizing current	16.7 A
cosϕ—Power factor	0.85
P_m—Nominal power	736 kW
f_e—Nominal electrical frequency	50 Hz
w_n—Nominal mechanical speed	1485 rpm
T_n—Nominal torque	4800 Nm
J_e—Electric motor inertia	17 kgm^2
N—Number of poles	4
R_s—Stator resistance	0.329 Ω
R_r—Rotor resistance	0.316 Ω
L_{ls}—Stator leakage inductance	16.4 mH
L_{lr}—Rotor leakage inductance	25.7 mH
Lm—Magnetizing inductance	0.7105 H
Td—Deadtime error	7 µs
Vdc—DC bus voltage	10.942 kV
fsw—Switching frequency	610 Hz
Inverter type	NPC 3-level

As mentioned in the introduction, apart from the several advantages offered by the V/Hz control strategy, the use of such an open-loop control introduces instability in its operations causing huge oscillations in motor currents and torque.

To demonstrate the problem of the current and torque oscillations with the conventional V/Hz control, an initial test was carried out where the motor (parameters in Table 1) was accelerated to the rated speed of 157.08 rad/s in 5 s (acceleration of 31.42 rad/s^2) at no load. From Figures 3–5, which show the stator phase A current, the mechanical speed, and the mechanical torque, respectively, it is evident that using the conventional V/Hz control for the motor introduces very large oscillations that are very harmful to the electrical drive if not compensated. In addition, with the fact of having a high power induction motor, mechanical problems such as possible shaft damages can also occur due to these large sustained oscillations. Furthermore, it should be noted that a high-power induction motor was chosen for this study since they experience more significant oscillations, which causes greater problems to the electrical and mechanical components of the system.
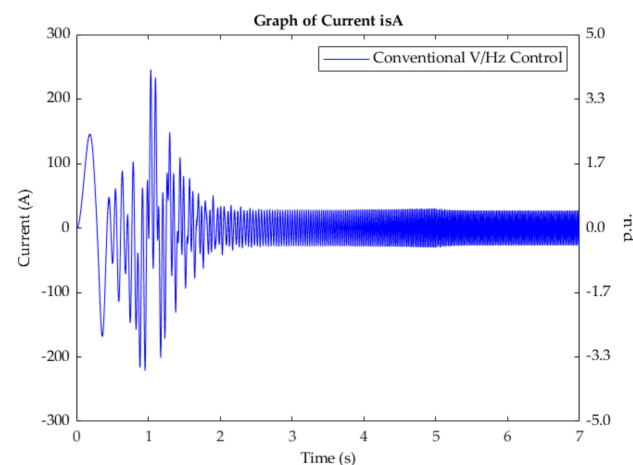

Figure 3. Phase A stator current, conventional V/Hz control, (0–50 Hz).
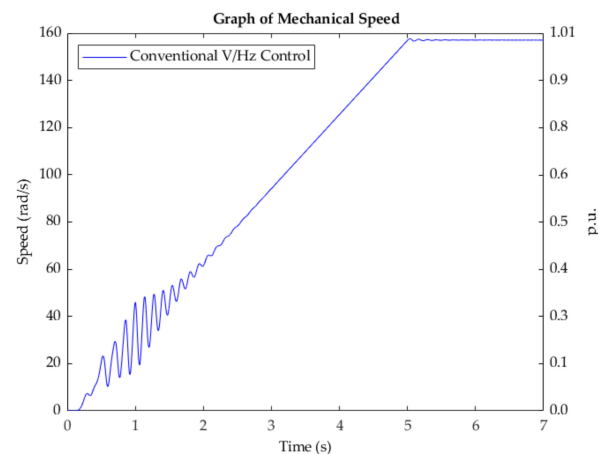
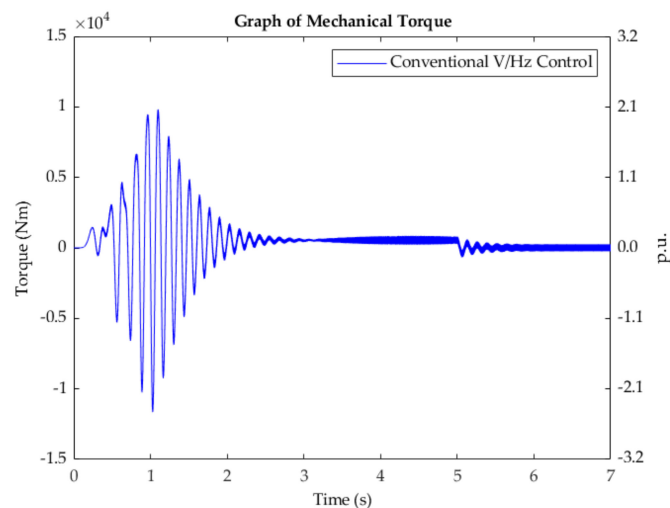**Figure 4.** Mechanical speed, conventional V/Hz control, (0–50 Hz).

Figure 5. Mechanical torque, conventional V/Hz control, (0–50 Hz).

Hence, in the following section of the article, a methodology is presented on how the instability region of an inverter-fed motor controlled with the conventional V/Hz technique can be predicted. With such a prediction of the instability region, effective mitigation techniques can be applied to counteract these oscillations in the currents and torque.

3. Mathematical Modelling

For the study of the instability region, the standard dynamic 5th order model was employed in the synchronous d-q reference frame, since it is commonly used for these analyses, and it is easy to implement. The following equations were used both to synthetize the proposed control and to simulate the model in the MATLAB/Simulink environment. Moreover, a three-voltage level NPC inverter was implemented in Simulink to drive the motor. As these equations are nonlinear in nature, for the purpose of this study, the system was linearized around a steady operating point in order to obtain the small-signal model of the inverter-fed induction motor presented in [13].

The small-signal model of the induction motor can be represented as:

$$\Delta \dot{x} = A \Delta x + B \Delta u \tag{1}$$

where:

$$\Delta x = \begin{bmatrix} \Delta i_{qs} \\ \Delta i_{ds} \\ \Delta i_{qr}' \\ \Delta i_{dr}' \\ \Delta w_r \end{bmatrix}, \quad \text{and} \quad \Delta u = \begin{bmatrix} \Delta V_{qs,id} \\ \Delta V_{ds,id} \\ 0 \\ 0 \\ \Delta T_l \end{bmatrix} \tag{2}$$

i_{qs} and i_{ds} are the q axis and d axis component of the stator current; v_{qs} and v_{ds} are the stator voltages in the q and d axis; i_{qr} and i_{dr} are the q and d axis components of the rotor current referred to the stator; w_r is the electrical speed of the rotor; and T_l is the load torque. In order to carry out the stability analysis, the system matrix A is defined as follows.

$$A = \begin{bmatrix} -\begin{bmatrix} l_s & 0 & l_m & 0 \\ 0 & l_s & 0 & l_m \\ l_m & 0 & l_r' & 0 \\ 0 & l_m & 0 & l_r' \end{bmatrix}^{-1} \begin{bmatrix} r_s + r_{q,eq0} & w_{s0}l_s - x_{qd,eq0} & 0 & w_{s0}l_m \\ -(w_{s0}l_s + x_{qd,eq0}) & r_s + r_{d,eq0} & -w_{s0}l_m & 0 \\ 0 & (w_{s0} - w_{r0})l_m & r_r' & (w_{s0} - w_{r0})l_r' \\ -(w_{s0} - w_{r0})l_m & 0 & -(w_{s0} - w_{r0})l_r' & r_r' \end{bmatrix} & -\begin{bmatrix} l_s & 0 & l_m & 0 \\ 0 & l_s & 0 & l_m \\ l_m & 0 & l_r' & 0 \\ 0 & l_m & 0 & l_r' \end{bmatrix}^{-1} \begin{bmatrix} 0 \\ 0 \\ -(l_m i_{ds0} + l_r' i_{dr0}') \\ (l_m i_{qs0} + l_r' i_{qr0}') \end{bmatrix} \\ \frac{3}{2J}\left(\frac{poles}{2}\right)^2 \begin{bmatrix} l_m i_{dr0}' \\ -l_m i_{qr0}' \\ -l_m i_{ds0} \\ l_m i_{qs0} \end{bmatrix}^T & \frac{-B}{J} \end{bmatrix} \tag{3}$$

In the system matrix A defined in Equation (3), the parameters, w_{s0}, w_{r0}, and B represent the stator synchronous speed, the mechanical speed, and the friction constant, respectively. It should be noted that the parameters with a subscript "0" represent a steady-state value. Appendix A of [13] contains a detailed theoretical description of the deadtime modelling. The equations used to calculate the terms arising due to the deadtime are as follows:

$$R_{eq0} = \frac{|\overrightarrow{V}_{s,err,f}|}{\sqrt{i_{qs0}^2 + i_{ds0}^2}} \tag{4}$$

R_{eq0} is the equivalent resistance as an effect of the deadtime where $|\overrightarrow{V}_{s,err,f}|$, defined in Equation (5) represents the magnitude of the deadtime error voltage.

$$|\overrightarrow{V}_{s,err,f}| = {}^4\!/_\pi\, V_{dc} T_d f_{sw} \tag{5}$$

This deadtime error voltage is calculated with the use of the dc bus voltage, V_{dc}, the inverter dead time, T_d, and the inverter switching frequency f_{sw}. It should be noted that the deadtime contributes to both the d and q axes components of the resistances ($R_{q,eq0}$ and $R_{d,eq0}$). Additionally, due to the deadtime, additional cross-coupling reactance ($X_{qd,eq0}$) was introduced in [13]. Equations (6)–(8) represent the terms arising from the effect of the inverter deadtime.

$$R_{q,eq0} = R_{eq0}\left(\frac{i_{ds}^2}{i_{qs}^2 + i_{ds}^2}\right) \tag{6}$$

$$R_{d,eq0} = R_{eq0}\left(\frac{i_{qs}^2}{i_{qs}^2 + i_{ds}^2}\right) \tag{7}$$

$$X_{qd,eq0} = R_{eq0}\left(\frac{i_{qs0}i_{ds0}}{i_{qs}^2 + i_{ds}^2}\right) \tag{8}$$

Utilizing the system matrix A defined in Equation (3), the root locus of the 736 kW induction motor drive with a frequency range of 0–50 Hz, a DC bus voltage of 10.942 kV, a switching frequency of 610 Hz, and a deadtime of 7 μs was obtained and is shown in Figure 6. The simulation was carried out with a V/Hz ratio of 1 p.u. In Table 1, the list of parameters of the motor used for the study and simulations are presented. Since a 5th order model of the induction machine was utilized, the five curves/lines shown in the plot represent the eigenvalues of the system. With this plot of the root locus, the speed range

that falls in the region of instability (eigenvalues on the right-hand side of the imaginary axis) can be easily identified.
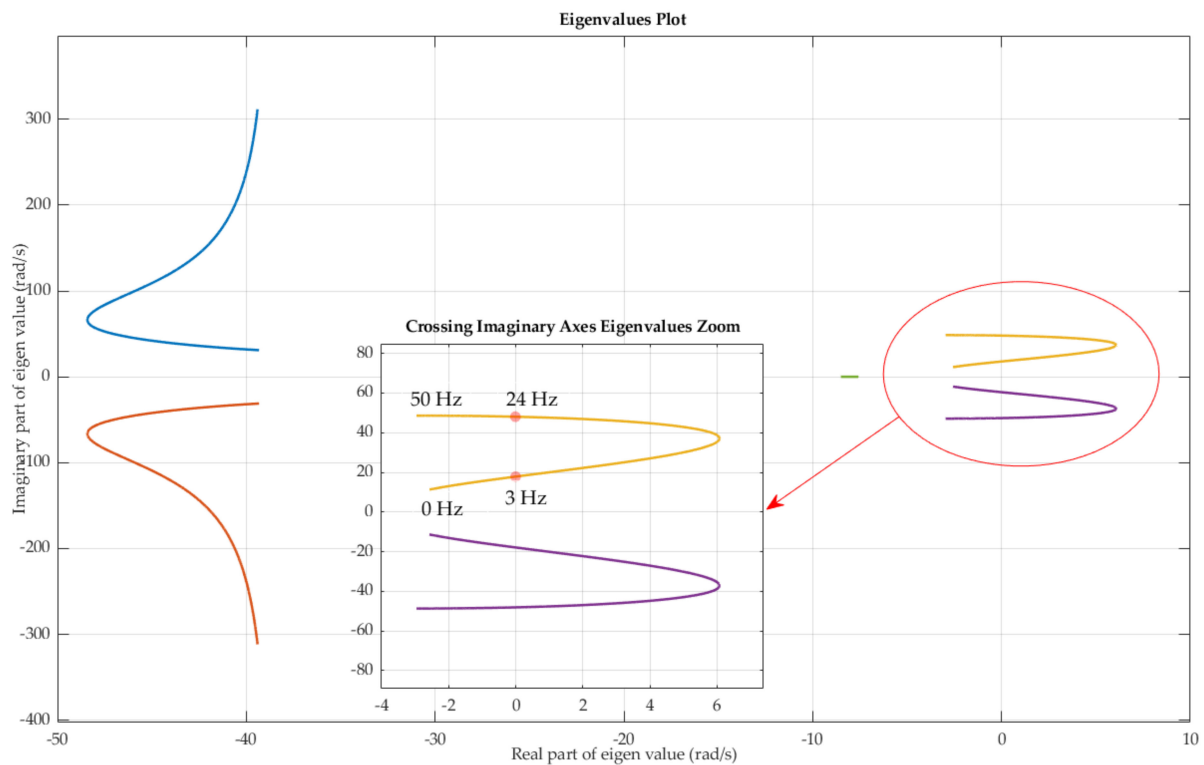

Figure 6. Locus of the eigenvalues of the 736 kW induction motor drive for a V/Hz ratio of 1 p.u. with a frequency range of 0–50 Hz, a DC bus voltage of 10.942 kV, a switching frequency of 610 Hz, and a deadtime of 7 μs.

From the root locus plot in Figure 6, it is clear to see that there are two points where the eigenvalues intersect the imaginary axis as labeled in the inset of the plot. Between these two points lies the region of instability for the particular V/Hz ratio (1 p.u. in this case). Hence, the speed range that lies in the instability region as per Figure 6 was between 3—24 Hz.

In order to achieve a better understanding, the region of instability was plotted in the V–f plane. Moreover, to obtain the region of instability of the machine as shown in Figure 7, the starting V/Hz ratio of 1 p.u. was gradually reduced until an inferior limit ratio was obtained. It can be observed from Figure 7 that the highest V/Hz ratio of 1 p.u. and the lowest V/Hz ratio was obtained yielding no instability. In this case, the lowest V/Hz ratio was 0.06 p.u. Referring to the ratio of 1 p.u., the two blue circles in Figure 7 represent the speed range of instability shown in Figure 6, which was 3–24 Hz.
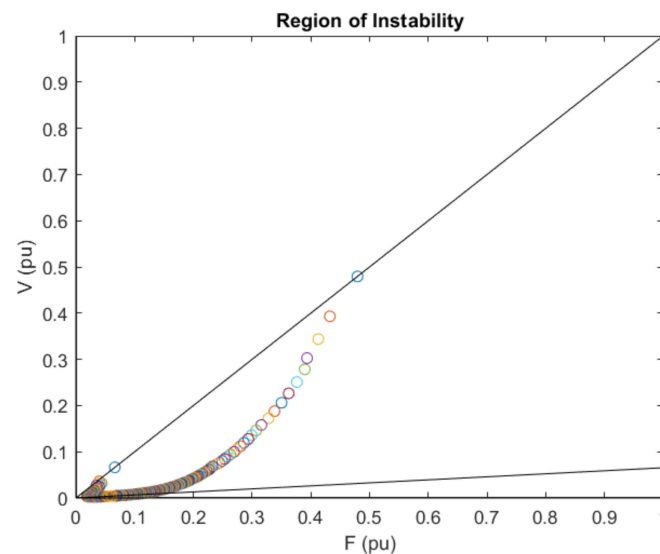
Figure 7. Region of instability in the V/f plane, (1 p.u.—0.06 p.u. V/Hz ratio).

4. Currents and Torque Oscillations Mitigation Techniques

As discussed in the previous sections of the article, using the conventional V/Hz strategy for the control of induction motors introduces very large oscillations in the currents and torque. However, since the methodology presented in the previous section enables one to predict the region of instability of the V/Hz controlled induction motors, effective mitigation techniques beforehand to avoid such harmful oscillations are possible to be implemented. In this section of the article, the authors present two mitigation techniques where the oscillations seen in the conventional V/Hz control are significantly reduced avoiding instability. In the first mitigation strategy, a novel oscillation suppression technique is proposed where a varying V/Hz slope ramp is utilized. In the second mitigation strategy, a variation of the active damping method presented in [16] is considered. The software MATLAB/Simulink was used to carry out the simulation tests.

4.1. Ad-Hoc Slope Ramping Algorithm (AHSRA)

This section presents a novel method to avoid the machine to operate inside the instability region as predicted in Section 3 and to suppress the oscillations in currents and torque. In this mitigation technique, named the Ad-Hoc Slope Ramping Algorithm (AHSRA) by the authors, instead of operating the induction motor with the rated V/Hz ratio (i.e., 1 p.u.), the V/Hz ratio is varied along with the different speed ranges of the induction motor. Having a V/Hz ratio of less than 1 p.u. is made possible since the motor is operated at a no-load condition. The different V/Hz ratios for different speed ranges are derived based on the graph of the region of instability plotted in the V–f plane. This is very well depicted in Figure 8, which shows the path (illustrated by the red arrows) of the V/Hz ratio taken for the control of the induction motor by avoiding the instability region as predicted from the methodology presented in Section 3 of the article.
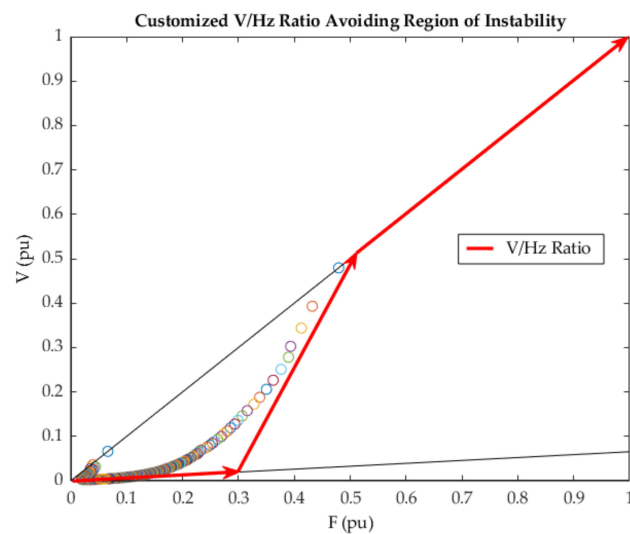
Figure 8. Customized V/Hz ratio to mitigate oscillations avoiding unstable operating points.

In order to obtain the varying V/Hz ratio based on the graph of the region of instability, the voltage and the reference speed were chosen in such a way that avoids the operation of the induction motor in the region of instability. Doing this allows the use of a unique slope ramp for different speed ranges thus avoiding the oscillations to occur. Figure 9 shows the voltage and reference speed adopted in the AHSRA.
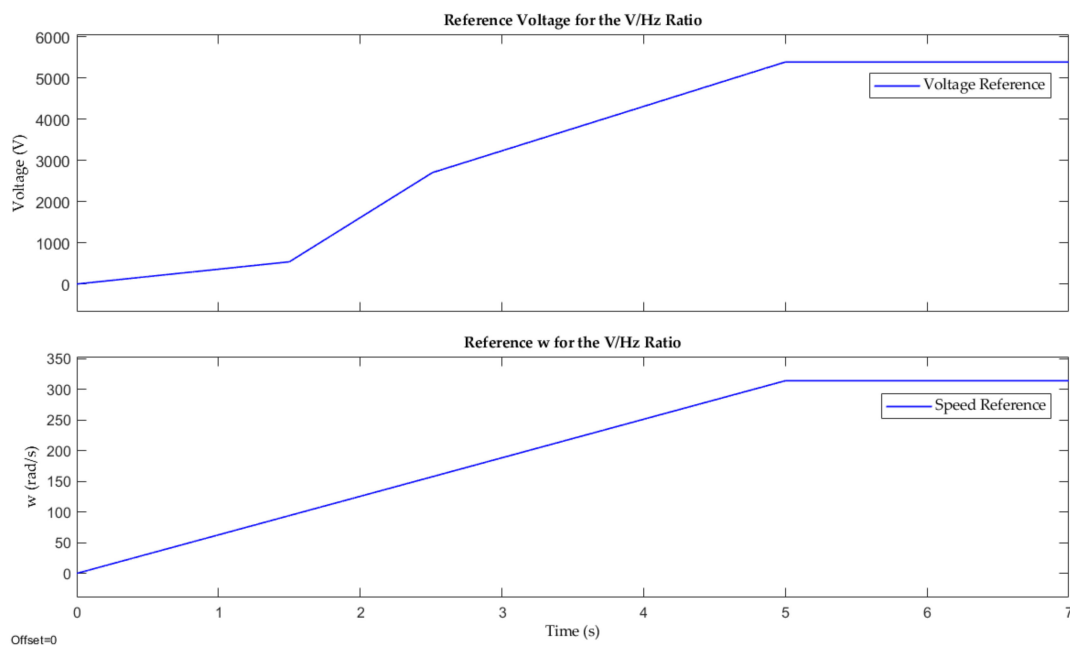

Figure 9. Customized voltage and w for AHSRA (proposed V/Hz control).

By applying AHSRA to the conventional V/Hz control, a significant reduction in the oscillations originally present was achieved. This is evident from Figures 10–12, which show the comparison of the stator currents, the mechanical speed, and the mechanical torque with and without the mitigation technique, respectively.
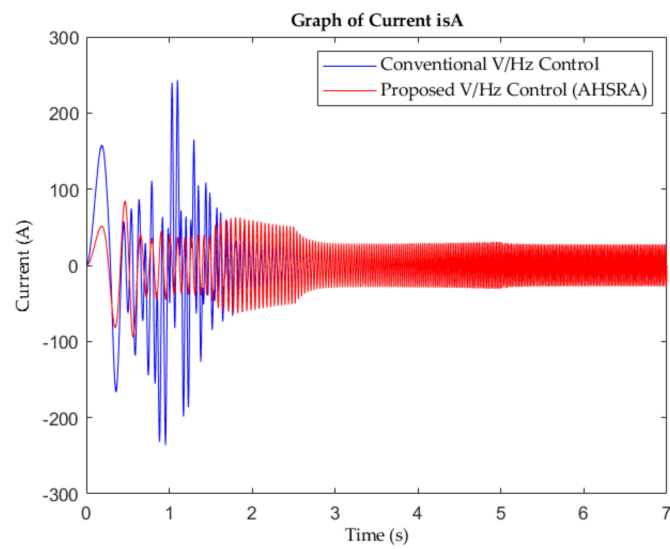
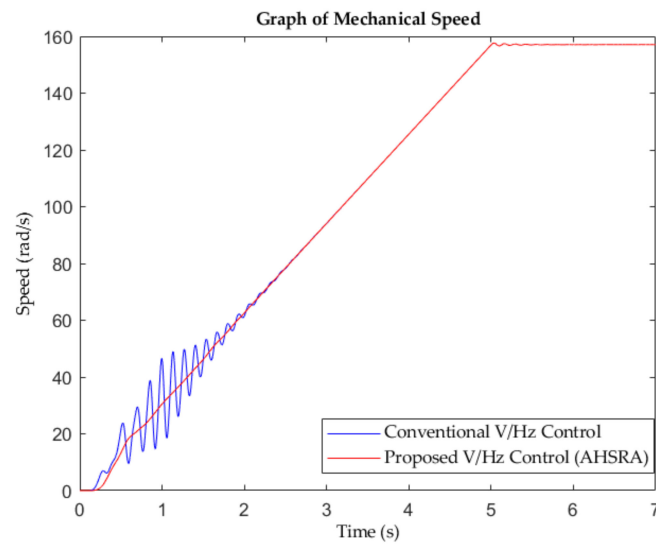**Figure 10.** Stator phase A current i_{sA}—ASHRA (red) vs. conventional V/Hz (blue).

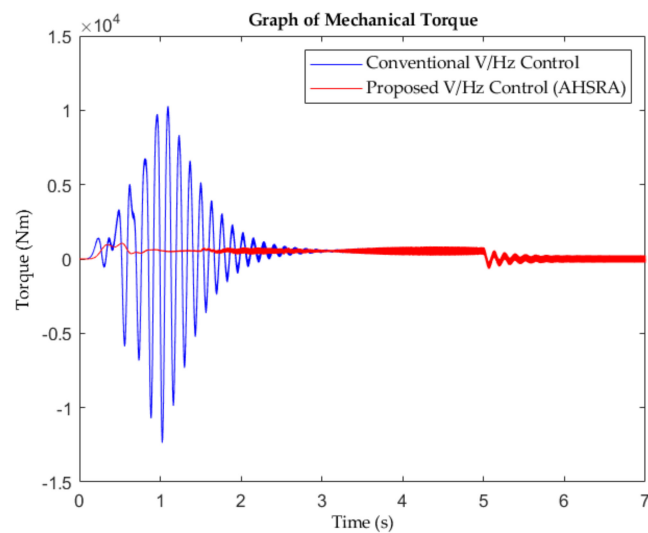**Figure 11.** Mechanical speed—AHSRA (red) vs. conventional V/Hz (blue).

Figure 12. Mechanical torque—AHSRA (red) vs. conventional V/Hz (blue).

4.2. Active Damping Strategy

The second proposed mitigation technique for suppressing current and torque oscillations is based on the active damping strategy presented in [16]. In order to shift all poles of the system to the left side part of the complex plane, a current feedback loop was adopted to obtain a correction factor, which was subtracted from the speed reference. Hence, in this technique, the damping functions compensate for the current oscillations by correcting only the speed reference. The value by which this correction is obtained is calculated from the d and q axis components of the stator current. Figure 13 represents the logic implemented to compensate for the current and torque oscillations. It shows that the three-phase measured stator currents are transformed into the synchronous d-q reference frame. Then, the two stator current components i_{sd} and isq were utilized in obtaining the speed correction factor. Enclosed in the red box in the figure are the two damping functions used for this purpose. In this article, a variation of this active damping strategy is proposed, where both the voltage and the speed reference of the V/Hz control are obtained using the correction factor resulting from the active damping functions, whereas in [16] only the speed reference is corrected with the output of the damping functions.
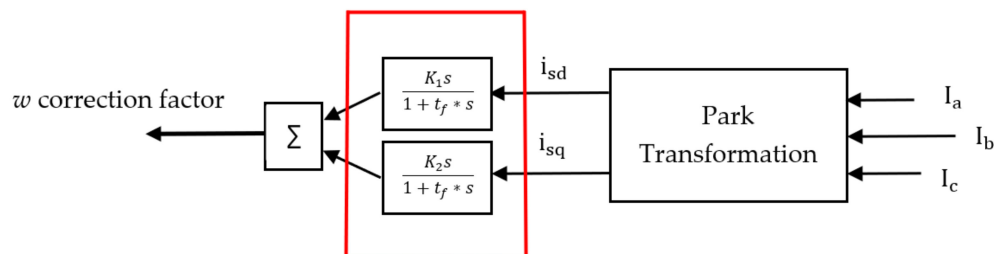

Figure 13. Damping logic implementation block diagram.

The active damping function was realized with the following transfer function:

$$\text{Out} = K_i \frac{s}{1 + T_f s} \text{In} \tag{9}$$

This transfer function consists of a derivative part and a first-order low pass filter with a time constant t_f and the two gains K_1 and K_2. The derivative part eliminates the continuous component of the signal, while the low pass filter isolates the low-frequency components. "In" is the d and q-axis component of the stator current, and "Out" is the speed reference correction factor. The outputs of the two active damping functions were summed together, giving the reference correction factor. This was then subtracted from the speed reference of the V/Hz to obtain the new voltage and speed references and to counteract the oscillation. In order to obtain the parameters (K_1, K_2), the linearised system matrix A defined in Equation (3) was modified by including the two active damping functions. This introduces two additional poles to the system, and the stability analysis carried out in Section 3 was repeated to select the values of K_1 and K_2, which shift the eigenvalues to the left-side of the complex plane. The purpose of the parameter t_f is to attenuate the high frequencies that would excite the oscillations in the system, and it was chosen through a heuristic approach. The parameters used in the design of the active damping function are listed in Table 2.

Table 2. Active damping function design parameters.

Parameter	Value
K_1	0.282
K_2	0.1225
t_f	2.1

To compare the results between the conventional V/Hz control and the V/Hz control with the proposed active damping functions to mitigate the current and torque oscillations, Figures 14–16 are shown. In Figure 14, a comparison between the phase A stator current is shown with and without the mitigation technique. From this, it is notable that the mitigation technique was very effective in counteracting the oscillations previously present. This is also evident in Figures 15 and 16, which illustrate a comparison between the mechanical speed and the mechanical torque, respectively, with and without the implementation of the mitigation technique. The very large oscillations that were present in these two graphs of the conventional V/Hz control were removed, except for the spike still present in the torque in Figure 16 in the very beginning of the speed ramp, and the motor was seen to be operating in a stable region.
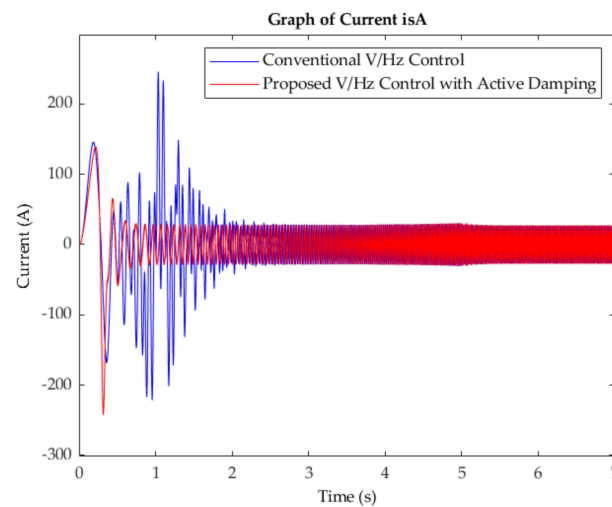

Figure 14. Stator phase A current i_{sA}—active damping technique (red) vs. conventional V/Hz (blue).
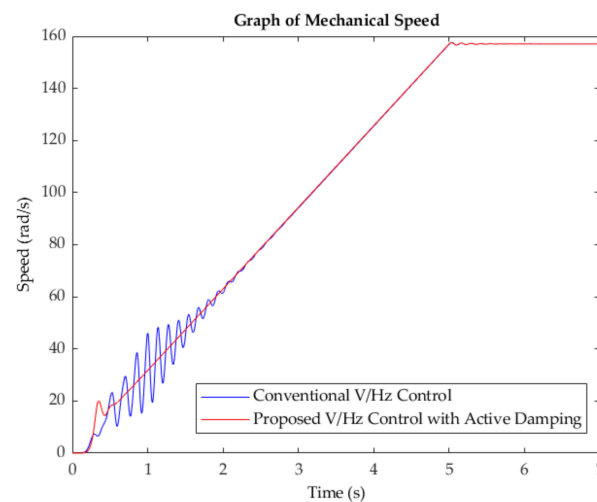

Figure 15. Mechanical speed—active damping technique (red) vs. conventional V/Hz (blue).
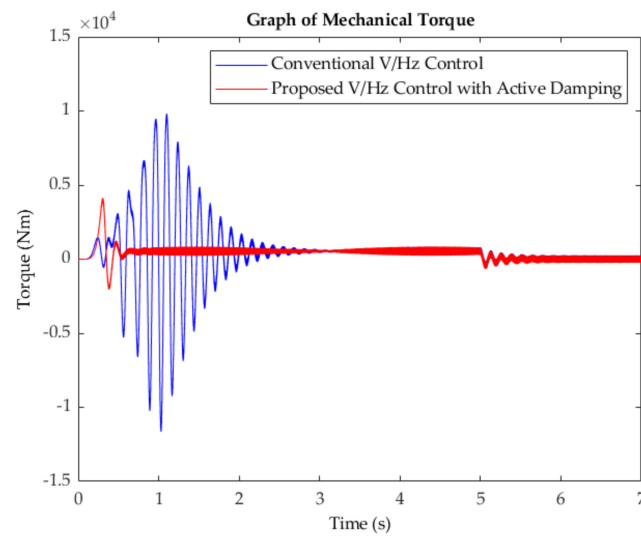
Figure 16. Mechanical torque—active damping technique (red) vs. conventional V/Hz (blue).

4.3. Mitigation Techniques Comparison (AHSRA vs. Active Damping)

The performances of the two mitigation techniques discussed above were compared, and the results are shown in Figures 17–19. In Figure 17, a comparison between the phase A stator current is shown for mitigation technique 1 (AHSRA) and mitigation technique 2 (active damping). From such a comparison, it is clearly evident that both the mitigation techniques were able to effectively suppress the oscillations present. In addition, it can also be seen that by using the ASHRA technique a better performance was obtained at the start of the simulation when compared to the active damping technique. A comparison between the mechanical speed and the mechanical torque obtained using the two mitigation techniques is presented in Figures 18 and 19, respectively. In both the figures, the effectiveness of the two mitigation techniques is clearly visible, and, similar to the current comparison, a better performance was also achieved at the start of the simulation for both the mechanical speed and the mechanical torque of the machine when using the ASHRA method.
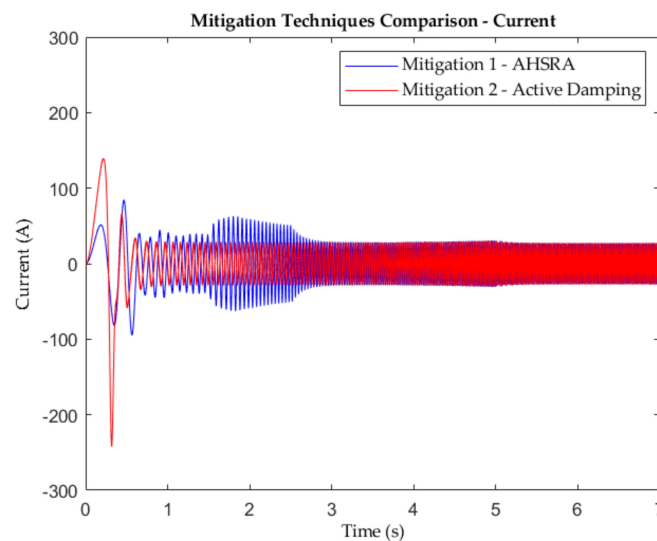

Figure 17. Stator phase A current i_{sA}—AHSRA (blue) vs. active damping technique (red).
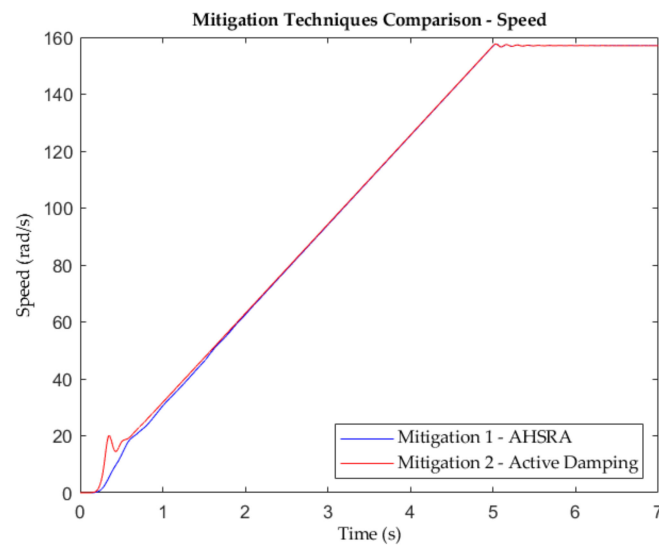
Figure 18. Mechanical speed—AHSRA (blue) vs. active damping technique (red).
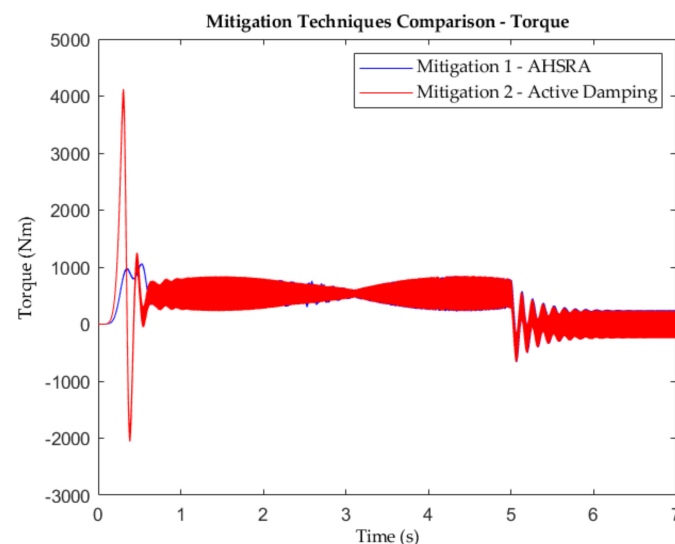

Figure 19. Mechanical torque—AHSRA (blue) vs. active damping technique (red).

5. Conclusions

In this article, the stability analysis of open-loop V/Hz controlled induction motors was presented. Firstly, the problem of high current and torque oscillations in the conventional V/Hz control of induction motors was introduced to the readers. A methodology was then presented that was used to predict the regions of instability during the control of the motor using the conventional V/Hz technique. The stability analysis of the induction motor was carried out using the derived system matrix A of the induction motor. To determine the region of instability, the eigenvalues of the induction motor with a speed range of 0–50 Hz were plotted. Hence, the eigenvalues that fell on the right-hand side of the imaginary axis were considered to calculate the speed range in which instability is obtained. For a better understanding, the region of instability region was plotted in the V–f plane, which made it easier to analyze the V/Hz ratio to use to avoid the oscillations during the operation of the induction motor. Two mitigation techniques were then proposed by the authors to compensate for the oscillations in the motor torque and currents. The first mitigation technique consists of a novel use of a varying V/Hz ratio instead of the rated V/Hz ratio. Doing this allows the user to avoid the operation of the motor in the region of instability, which was proven through the simulation results discussed in the article. The

second mitigation technique, which is a variation of the method presented in [16], proposed the use of two damping functions to counteract the oscillations by correcting the value of the speed reference. The speed reference correction factor was calculated using the two damping functions and the d and q axis components of the stator current. The results of the second mitigation technique were also validated through simulation results discussed in the article. A comparison of the two proposed methods is shown in Figures 17–19. Finally, it can be said that with the ability of being able to effectively predict the region of instability in the open-loop V/Hz control of induction motors, it is possible to avoid the problem of high oscillations in the currents and torque by implementing such mitigation techniques as presented in the article.

Author Contributions: Conceptualization, M.M. and L.V.; data curation, K.K. and S.C.; formal analysis, L.V. and M.P.; methodology, L.V., K.K., S.C. and M.P.; software, K.K., S.C. and L.C.; supervision, M.M. and L.V.; validation, L.V. and M.M.; writing—original draft, K.K., S.C. and L.C.; writing— review and editing, M.M., M.P. and L.V. All authors have read and agreed to the published version of the manuscript.

References

1. Dems, M.; Komeza, K.; Szulakowski, J.; Kubiak, W. Dynamic Simulation of High-Speed Induction Motor. *Energies* **2021**, *14*, 2713. [CrossRef]
2. Shenai, K.; Scott, R.; Baliga, B. Optimum semiconductors for high-power electronics. *IEEE Trans. Electron Devices* **1989**, *36*, 1811–1823. [CrossRef]
3. Faranda, R.; Hafezi, H.; Akkala, K.; Lazzaroni, M. AC "Back to Back" Switching Device in Industrial Application. *Energies* **2020**, *13*, 3539. [CrossRef]
4. Abouzeid, A.F.; Guerrero, J.M.; Endemaño, A.; Muniategui, I.; Ortega, D.; Larrazabal, I.; Briz, F. Control Strategies for Induction Motors in Railway Traction Applications. *Energies* **2020**, *13*, 700. [CrossRef]
5. Xiang, Y. Instability compensation of V/Hz PWM inverter-fed induction motor drives. In Proceedings of the IAS '97. Conference Record of the 1997 IEEE Industry Applications Conference Thirty-Second IAS Annual Meeting, New Orleans, LA, USA, 5–9 October 1997; Institute of Electrical and Electronics Engineers (IEEE): Piscataway, NJ, USA, 2002; Volume 1, pp. 613–620.
6. Lipo, T.A.; Krause, P.C. Stability Analysis of a Rectifier-Inverter Induction Motor Drive. *IEEE Trans. Power Appar. Syst.* **1969**, *PAS-88*, 55–66. [CrossRef]
7. Ueda, R.; Sonoda, T.; Ichikawa, M.; Koga, K. Stability analysis in induction motor driven by V/f controlled general purpose inverter. In Proceedings of the Conference Record of the 1990 IEEE Industry Applications Society Annual Meeting, Vancouver, BC, Canada, 10–14 October 1990; Institute of Electrical and Electronics Engineers (IEEE): Piscataway, NJ, USA, 2002; Volume 1, pp. 365–372.
8. Vladimir, K.; Alexander, A. On the Physical Nature of Frequency Control Problems of Induction Motor Drives. *Energies* **2021**, *14*, 4246. [CrossRef]
9. Hinkkanen, M.; Tiitinen, L.; Molsa, E.; Harnefors, L. On the Stability of Volts-per-Hertz Control for Induction Motors. *IEEE J. Emerg. Sel. Top. Power Electron.* **2021**, *1*. [CrossRef]
10. Lin, J.-L. A new approach of dead-time compensation for PWM voltage inverters. *IEEE Trans. Circuits Syst. I Regul. Pap.* **2002**, *49*, 476–483. [CrossRef]
11. Cheng, J.; Chen, D.; Chen, G. Modeling and Compensation for Dead-Time Effect in High Power IGBT/IGCT Converters with SHE-PWM Modulation. *Energies* **2020**, *13*, 4348. [CrossRef]
12. Colby, R.; Simlot, A.; Hallouda, M. Simplified model and corrective measures for induction motor instability caused by PWM inverter blanking time. In Proceedings of the 21st Annual IEEE Conference on Power Electronics Specialists, San Antonio, TX, USA, 6 August 2002; Institute of Electrical and Electronics Engineers (IEEE): Piscataway, NJ, USA, 2002; pp. 678–683.
13. Guha, A.; Narayanan, G. Small-Signal Stability Analysis of an Open-Loop Induction Motor Drive Including the Effect of Inverter Deadtime. *IEEE Trans. Ind. Appl.* **2016**, *52*, 242–253. [CrossRef]
14. Mutoh, N.; Ueda, A.; Sakai, K.; Hattori, M.; Nagato, Y. Stabilizing control methods for suppressing oscillations of induction motors driven by PWM inverters. In Proceedings of the 1985 IEEE Power Electronics Specialists Conference, Toulouse, France, 24–28 June 1985; Volume 37, pp. 48–56. [CrossRef]
15. Mosskull, H. Some issues on stabilization of an induction machine drive. In Proceedings of the 2004 43rd IEEE Conference on Decision and Control (CDC) (IEEE Cat. No.04CH37601), Nassau, Bahamas, 14–17 December 2004; Institute of Electrical and Electronics Engineers (IEEE): Piscataway, NJ, USA, 2004; Volume 4, pp. 4441–4446.

16. Qian, Z.; Yao, W.; Lee, K. Stability analysis and improvement of V/Hz controlled adjustable speed drives equipped with small DC-link thin film capacitors. In Proceedings of the 2018 IEEE Applied Power Electronics Conference and Exposition (APEC), San Antonio, TX, USA, 4–8 March 2018; Institute of Electrical and Electronics Engineers (IEEE): Piscataway, NJ, USA, 2018; pp. 861–866.
17. Lee, K.; Yao, W.; Chen, B.; Lu, Z.; Yu, A.; Li, D. Stability Analysis and Mitigation of Oscillation in an Induction Machine. *IEEE Trans. Ind. Appl.* **2014**, *50*, 3767–3776. [CrossRef]
18. Kumar, K.; Marchesoni, M.; Maule, Z.; Passalacqua, M.; Soso, F.; Vaccaro, L. Currents and Torque Oscillations Mitigation in High Power Induction Motor Drives. In Proceedings of the 2021 IEEE 15th International Conference on Compatibility, Power Electronics and Power Engineering (CPE-POWERENG), Florence, Italy, 14–16 July 2021; Institute of Electrical and Electronics Engineers (IEEE): Piscataway, NJ, USA, 2021; pp. 1–5.